International Journal of Bifurcation and Chaos, Vol. 13, No. 1 (2003) 147–161

THE MALKUS–ROBBINS DYNAMO WITH A LINEAR SERIES MOTOR

IRENE M. MOROZ
Mathematical Institute,
24-29 St Giles', Oxford OX1 3LB, UK
moroz@maths.ox.ac.uk

Received July 26, 2001; Revised October 31, 2001

Hide [1997] has introduced a number of different nonlinear models to describe the behavior of n-coupled self-exciting Faraday disk homopolar dynamos. The hierarchy of dynamos based upon the Hide *et al.* [1996] study has already received much attention in the literature (see [Moroz, 2001] for a review). In this paper we focus upon the remaining dynamo, namely Case 3 of [Hide, 1997] for the particular limit in which the Malkus–Robbins dynamo [Malkus, 1972; Robbins, 1997] obtains, but now modified by the presence of a linear series motor. We compare and contrast the linear and the nonlinear behaviors of the two types of dynamo.

Keywords: Dynamos; bifurcations.

1. Introduction

In a recent paper Hide [1997] derived two classes of n-coupled self-exciting Faraday disk homopolar dynamos. The first class is based upon the original Hide *et al.* [1996] model in which a Faraday disk is connected in series with a coil and an electric motor, through which flows a current $x(t)$. The disk is rotated with angular speed $y(t)$ by the action of a steady applied couple α, while the armature of the motor rotates with angular speed $z(t)$. There is mechanical friction in both the disk and the motor, parameterized by κ and λ, respectively. The moment of inertia of the armature is given by β.

Hierarchies of this dynamo are constructed by arranging the units in either a lattice or a ring, connecting the coil of dynamo j to the disk of dynamo (see [Hide, 1997] for further details of the construction and for the $n = 2$ configuration). This class of dynamos has already received a lot of attention in the literature ([Moroz *et al.*, 1998a, 1998b; Hide & Moroz, 1999; Goldbrum *et al.*, 2000; Skeldon & Moroz, 1998; Hide, 1998; Moroz & Hide, 2000; Moroz, 2001b, 2001c]) and will not be discussed in any detail here. Instead we focus upon the second class of dynamo of which a prototype comprises a single Faraday disk and coil configuration, connected in series with three electric motors (see [Hide, 1997] Fig. 1 for a schematic).

In the single disk dynamo, the motors E_r, E_a and E_c are driven into rotation with nondimensional time-dependent angular speeds z_c, z_a and z_r, respectively by the currents flowing through the unit. For each motor, one of the terminals meets at a common junction while the other is connected as follows: E_r to the rim of the disk via a brush; E_a to the axle of the disk via a brush; E_c to the axle of the disk via the coil. E_r and E_c are in series, while E_a is in parallel to E_c and to the coil. A nondimensionalized current $x_c + x_a$ flows through E_r, where x_c is the current through E_c, and x_a is that through E_a. The governing equations take the form (see [Hide, 1997] for a complete derivation)

$$(1 + l_r)\dot{x}_c + l_r\dot{x}_a = x_c(y - 1 - r_r) - r_r x_a - \beta(z_c + h_r z_r)\,, \qquad (1a)$$

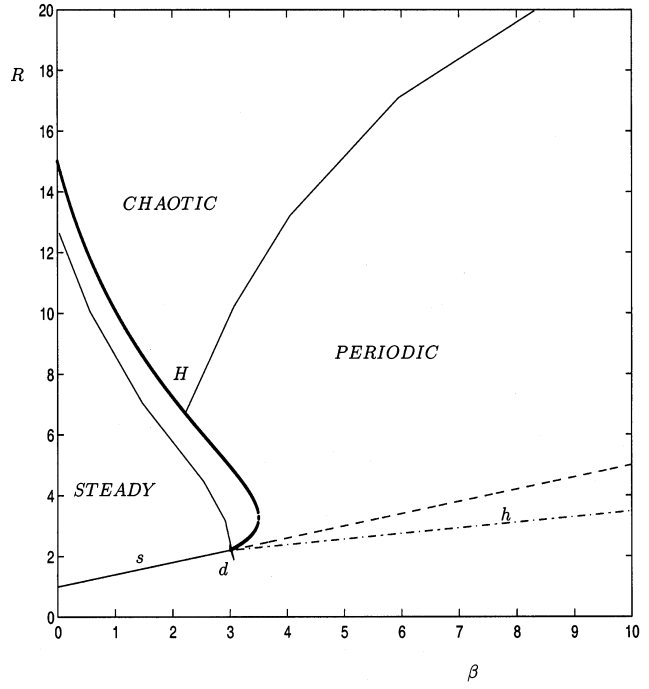

Fig. 1. Linear stability curves for case (i) with $\Lambda = 0.5$, $\sigma = 5$ and $\nu = 1$. The curves of steady and Hopf bifurcations from the trivial equilibrium state are denoted by s and h, respectively, while the Hopf bifurcation curve associated with the nontrivial states is denoted by H. The double-zero bifurcation is labeled as d. Also shown are the approximate nonlinear transition curves between steady and chaotic, and periodic and chaotic solutions.

$$\dot{x}_c - l_a\dot{x}_a = -x_c - \beta z_c + r_a x_a + h_a\beta z_a\,, \tag{1b}$$

$$\dot{y} = \alpha[1 - x_c(x_c + x_a)] - \kappa y\,, \tag{1c}$$

$$\dot{z}_c = x_c - \lambda z_c\,, \tag{1d}$$

$$b_a\dot{z}_a = h_a x_a - d_a\lambda z_a\,, \tag{1e}$$

$$b_r\dot{z}_r = h_r(x_c + x_a) - d_r\lambda z_r\,, \tag{1f}$$

where the definitions of the parameters are given in detail in [Hide, 1997]. In the discussion following the presentation of these equations, Hide [1997] notes that if the motors are replaced by elements with resistance and inductance only (so that $\beta = h_a = h_r = 0$), then (1) reduces to the Malkus–Robbins dynamo [Malkus, 1972; Robbins, 1997]. In this paper we investigate an extension to the Robbins analysis, where we also set $h_a = h_r = 0$ but now insist that $\beta \neq 0$, so that the motor E_c is still present in the special case where $l_a = 0$, which corresponds to case (b) studied by Robbins [1977].

The consequence of setting $h_a = h_r = 0$ is to decouple the evolution of z_a and z_r from the remaining equations so that, when all the parameters appearing in (1) are taken to be positive, z_a, $z_r \to 0$, and we are left with a reduced system of four coupled nonlinear equations. The additional requirement that $l_a = 0$ enables the simplest direct comparison with case (b) to be made. (In future work we shall relax this third assumption and so are able to investigate both cases (a) and (b) of [Robbins, 1977]). The simplified system we investigate is therefore

$$(1 + l_r)\dot{x}_c + l_r\dot{x}_a = x_c(y - 1 - r_r) - r_r x_a - \beta z_c\,, \tag{2a}$$

$$\dot{x}_c = -x_c - \beta z_c + r_a x_a\,, \tag{2b}$$

$$\dot{y} = \alpha[1 - x_c(x_c + x_a)] - \kappa y\,, \tag{2c}$$

$$\dot{z}_c = x_c - \lambda z_c\,. \tag{2d}$$

The paper is structured as follows. In Sec. 2 we briefly review that aspect of Robbins [1977] that is of relevance to our analysis, summarizing the bifurcation behavior found in the Malkus–Robbins dynamo. In Sec. 3 we apply as much of the same rescaling as possible that was used in [Robbins, 1977] to generate a set of equations which are readily identifiable as an extension to that model and then contrast the linear stability analysis with the corresponding analysis of [Robbins, 1977]. Section 4 describes selected numerical integrations of the four-mode system and we draw our conclusions in Sec. 5, indicating possible lines of future research.

2. The Transformed Dynamo Equations

As a prelude to a discussion of the four-mode dynamo (2) we summarize the key features of the Robbins' dynamo derivation and analysis.

2.1. *The Malkus–Robbins dynamo*

The Malkus–Robbins dynamo comprises a conducting disk, driven to rotate with angular speed $w(t)$ by a constant torque T, with a magnetic field normal to the disk inducing a radial e.m.f. (as in [Hide *et al.*, 1996]). A current $z(t)$ flowing in the disk, is removed by a ring of brushes and is fed to a coil and external load. The coil is aligned in such a way

that its current $y(t)$ produces a magnetic field to reinforce the original field.

The inductance of the coil, brushes and shunt are (L_c, L_b, L_s) and (B_c, B_b, B_s), respectively. Robbins [1977] notes that there are only two parameter regimes for which magnetic reversals are possible. The first, termed case (a), is when

$$L_c/B_c < L_s/B_s\,, \quad L_b/B_b < L_s/B_s$$

for which stable Van der Pol oscillations occur. The second (and the relevant regime here), case (b) has

$$L_c/B_c > L_s/B_s\,, \quad L_b/B_b > L_s/B_s$$

and with $L_s = 0$ is transformable to the Lorenz Strange Attractor equations.

For the sake of future comparisons, we note the following correspondences between the variables and the parameters in the Robbins dynamo and (1):

$$(L_s, B_s; L_b, B_b; L_c, B_c) \longleftrightarrow (l_a, r_a; l_r, r_r; 1, 1)$$

and

$$(w, z, y) \longleftrightarrow (y, x_c + x_a, x_c)\,.$$

Therefore setting $L_s = 0$ is equivalent to setting $l_a = 0$ and case (b) is equivalent to the requirement that $r_a > l_a$ and $l_r r_a > l_a r_r$.

The nondimensional form of the Malkus–Robbins dynamo is [Robbins, 1997]

$$\dot{w} = R - zy - \nu w\,, \tag{3a}$$

$$\dot{z} = wy - z\,, \tag{3b}$$

$$\dot{y} = \sigma(z - y)\,, \tag{3c}$$

where R, ν and σ are positive parameters which depend upon the physical characteristics of the components of the dynamo (the reader is referred to [Robbins, 1997] for a derivation of (3) as well as explanations of the parameters).

There are three equilibrium configurations:

$$\begin{aligned}&(w_0, z_0, y_0) = (R/\nu, 0, 0),\\ &(w_e, z_e, y_e) = (1, \pm\sqrt{(R-\nu)}, \pm\sqrt{(R-\nu)})\,.\end{aligned} \tag{4}$$

The first equilibrium in (4) corresponds to the zero field state, while the remaining two are finite amplitude states. A bifurcation analysis of the zero state shows that Hopf bifurcations are not possible; the only bifurcation is a pitchfork bifurcation to the remaining two equilibria when $R = \nu$. A bifurcation analysis of the finite amplitude states shows that a subcritical Hopf bifurcation occurs [Robbins, 1977] for

$$R_c = \sigma\nu\frac{\sigma + \nu + 3}{\sigma - 1 - \nu}\,. \tag{5}$$

Robbins has numerically integrated (3) for $\sigma = 5$ and $\nu = 1$ for various values of R. We note that for these values of σ and ν, $R_c = 15$. Irregular reversals occur for $R = 14.625$, while equilibration to a steady state occurs for $R = 14.25$ after an initial period of transient chaotic behavior.

In this paper, we shall use the same values for σ and ν as far as possible to facilitate direct comparisons between the two systems.

2.2. *The extended Robbins dynamo*

In order to recast (2) into a form reminiscent of (3), we introduce new variables

$$\begin{aligned}&y = AW - r_a\,, \quad x_c + x_a = BZ\,,\\ &x_c = CY\,, \quad z_c = DU\,, \quad t = T\tau\,,\end{aligned} \tag{6}$$

where

$$\begin{aligned}&A = \frac{(1 + r_a)(r_a + r_r)}{r_a}\,, \quad C = \frac{(r_a + r_r)}{\sqrt{l_r}},\\ &B = \frac{A}{\sqrt{l_r}}\,, \quad D = \sqrt{l_r}\,,\end{aligned} \tag{7}$$

with $T = l_r/(r_a + r_r)$. Then (2) reduces to

$$W' = R - \alpha ZY - \nu W\,, \tag{8a}$$

$$Z' = YW - Z\,, \tag{8b}$$

$$Y' = \sigma(Z - Y) - \hat{\beta}U\,, \tag{8c}$$

$$U' = Y - \Lambda U\,, \tag{8d}$$

where

$$\begin{aligned}&R = \frac{\nu^2 r_a}{\sigma\kappa(r_a + r_r)}(r_a + \overline{\alpha})\,, \quad \nu = \frac{\kappa l_r}{r_a + r_r}\,,\\ &\sigma = \frac{l_r(1 + r_a)}{r_a + r_r}\,, \quad \Lambda = \frac{\lambda l_r}{r_a + r_r}\,,\end{aligned} \tag{9}$$

$\overline{\alpha} = \alpha/\kappa$ and $\hat{\beta} = \nu^2\beta/\kappa^2$, with derivatives now being performed with respect to τ. A comparison of (3) with (8) identifies the latter as the extended version of the Malkus–Robbins dynamo, whose behavior we shall investigate in the next two sections.

We close this section with the following observation. If we make the transformation

$$(W, Z, Y, U) \to \alpha^{-1/2}(\alpha^{1/2}W, Z, Y, U)\,,$$

then Eqs. (8a)–(8d) are unchanged, except for the absence of α in (8a). As has been verified in both the bifurcation analysis of Sec. 3 and the numerical integrations of Sec. 4, the role that this α plays regarding the solutions of (8) is simply to rescale Z, Y and U. It has no qualitative effect whatsoever on the bifurcation sequences observed.

3. Bifurcation Analysis for the Extended Malkus–Robbins Dynamo

We now focus upon the extended Malkus–Robbins dynamo and identify both the equilibrium solutions and determine the principal bifurcations associated with them. We also compare our results with those for (3) as well as for the Hide *et al.* [1996] family of dynamo models whenever appropriate.

3.1. *The equilibrium solutions*

The extended Malkus–Robbins dynamo equations (7) are invariant under the transformation

$$(W, Z, Y, U) \to (W, -Z, -Y, -U)$$

and the equilibrium states reflect this symmetry. There are three equilibrium solutions:

$$\mathbf{W_0} = (W_0, Z_0, Y_0, U_0) = (R/\nu, 0, 0, 0)\,, \quad (10)$$

which we term the trivial equilibrium state and

$$\mathbf{W_e} = (W_e, W_e Y_e, Y_e, Y_e/\Lambda)\,, \quad (11)$$

where

$$W_e = 1 + \frac{\hat{\beta}}{\Lambda\sigma}\,, \quad Y_e = \pm\sqrt{\frac{R - \nu W_e}{\alpha W_e}}\,, \quad (12)$$

which we term the nontrivial equilibrium states.

Note that the trivial equilibrium state is identical to $(4)_{\rm a}$ (with the obvious absence of U), while the nontrivial equilibria (11) and (12) reduce to $(4)_{\rm b}$ when $\beta = 0$ and $\alpha = 1$.

3.2. *Bifurcations from the trivial state*

A linear stability analysis of (10) for perturbations $\propto e^{mt}$ yields a cubic characteristic equation for m, together with the separable root $m = -\nu < 0$:

$$m^3 + A_2 m^2 + A_1 m + A_0 = 0\,, \quad (13)$$

where

$$A_2 = 1 + \sigma + \Lambda\,, \quad (14a)$$

$$A_1 = \sigma(1 - R/\nu) + \Lambda(1 + \sigma) + \hat{\beta}\,, \quad (14b)$$

$$A_0 = \sigma\Lambda(1 - R/\nu) + \hat{\beta}\,. \quad (14c)$$

For ease of comparison with the Malkus–Robbins case, we treat R as the principal bifurcation parameter. In order to compare with the results of Hide *et al.* [1996], who chose α, we could of course use (9) to express R in terms of α. The essential details of the bifurcation analysis will then be unchanged; the only difference will be a rescaled and translated version of the results.

A steady bifurcation occurs when $A_0 = 0$ or

$$R_s = \nu\left(1 + \frac{\hat{\beta}}{\sigma\Lambda}\right) \quad (15)$$

and a Hopf bifurcation occurs when $A_1 A_2 = A_0$, provided $A_1 > 0$ and $A_0 > 0$ (A_2 is automatically positive), when

$$R_h = \frac{\nu(\sigma + \Lambda)}{\sigma(1 + \sigma)}[(1 + \sigma)(1 + \Lambda) + \hat{\beta}]\,, \quad (16)$$

with frequency given by $m = \pm i\omega$, where

$$\omega^2 = [\hat{\beta}(1 - \lambda) - \Lambda^2(1 + \sigma)]/(1 + \sigma)\,. \quad (17)$$

We see that $\omega^2 > 0$ provided $\hat{\beta} > \Lambda^2(1 + \sigma)/(1 - \Lambda)$. A double-zero Takens–Bogdanov bifurcation occurs when $A_0 = A_1 = 0$, so that

$$(R_d, \hat{\beta}_d) = \left(\frac{\nu(\Lambda + \sigma)}{\sigma(1 - \Lambda)}\,, \frac{\Lambda^2(1 + \sigma)}{1 - \Lambda}\right), \quad (18)$$

provided $\Lambda < 1$.

The above is in marked contrast to the bifurcation analysis for (3), where the only bifurcation possible for the zero state is the pitchfork bifurcation (corresponding to (15)). The presence of a motor (nonzero β and Λ terms) therefore means that additional bifurcations, similar to the Hide *et al.* [1996] problem, are now possible.

3.3. *Bifurcations from the nontrivial states*

We now consider the primary bifurcations that can arise from the nontrivial equilibria (11) and (12). Under perturbations of the form e^{st}, we now obtain a nonseparable quartic characteristic equation

$$s^4 + B_3 s^3 + B_2 s^2 + B_1 s + B_0 = 0\,, \qquad (19)$$

where

$$B_3 = 1 + \nu + \sigma + \Lambda\,, \qquad (20a)$$

$$B_2 = (1+\nu)(\sigma+\Lambda) + \sigma W_e(\Lambda - 1) + R/W_e\,, \qquad (20b)$$

$$B_1 = \nu\sigma(\Lambda - 2)W_e + R[\sigma + (\sigma+\Lambda)/W_e]\,, \qquad (20c)$$

$$B_0 = 2\sigma\Lambda(R - \nu W_e)\,. \qquad (20d)$$

From (19) and (20) we see that a steady bifurcation occurs when $B_0 = 0$, which can only occur for $W_e = R/\nu$. Comparison with (10) shows that this corresponds to the pitchfork bifurcation of the trivial equilibrium state. A double-zero bifurcation is also possible when $B_0 = B_1 = 0$. Substitution of $W_e = R/\nu$ into $B_1 = 0$ and use of $(12)_\mathrm{a}$ results in the same condition (18) as for the trivial equilibrium solution. Therefore the extended Malkus–Robbins dynamo is similar to the Hide *et al.* [1996] dynamo in the coincidence of the steady and double-zero bifurcations for the trivial and the nontrivial equilibrium states.

As in [Hide & Moroz, 1999], it is not possible to write down a simple elegant explicit formula for the onset of a Hopf bifurcation for the nontrivial equilibria. When $s = \pm i\Omega$, we can show that Hopf bifurcations occur along the curve

$$B_1^2 - B_1 B_2 B_3 + B_0 B_3^2 = 0\,, \qquad (21)$$

where Ω is the common root of:

$$\Omega^2 = \frac{B_2}{2} \pm \frac{1}{2}[B_2^2 - 4B_0]^{\frac{1}{2}} = \frac{B_1}{B_3}\,. \qquad (22)$$

Appendix A summarizes the method we used to compute the nontrivial Hopf bifurcation curve. Numerical calculations show that one end of the branch can terminate on the double-zero bifurcation point, while the other can terminate on the R axis (i.e. $\beta = 0$) at the precise value R_c given in [Robbins, 1997] for the onset of the subcritical Hopf bifurcation for the Malkus–Robbins nontrivial equilibrium state.

3.4. *Linear stability curves*

The bifurcation analysis described above and in [Robbins, 1997] suggests we consider four different parameter regimes:-

(i) $\Lambda < 1$ and $\sigma > 1 + \nu$;
(ii) $\Lambda > 1$ and $\sigma > 1 + \nu$;
(iii) $\Lambda < 1$ and $0 < \sigma < 1 + \nu$;
(iv) $\Lambda > 1$ and $0 < \sigma < 1 + \nu$.

From (18) we see that the conditions on Λ correspond to the existence or otherwise of the Takens–Bogdanov bifurcation and so the existence or otherwise of the bifurcating limit cycle which originates from this point [see (16) and (17)]. The conditions on σ relate to the termination or otherwise of this limit cycle on the subcritical Hopf bifurcation point (determined by the vanishing of the denominator in the definition of R_c in (5)). To illustrate the four cases, we chose four typical parameter values that are consistent with these inequalities and plot the linear stability curves in the (β, R)-plane for $r_r = 1$ and appropriate values of ν. Indeed in all the numerical integrations reported in this paper we set $\nu = \kappa = 1$, so that $\hat{\beta} = \beta$ throughout.

3.4.1. $\Lambda < 1$ *and* $\sigma > 1 + \nu$

As an example of the case when $\Lambda < 1$ and $\sigma > 1+\nu$, we choose $\Lambda = 0.5$, $\sigma = 5$ and $\nu = 1$. These choices for σ and ν coincide with those used in [Robbins, 1997] and, from (9), correspond to the choices of $\kappa/\lambda = 2$. Since $r_a = \sigma\kappa/\nu - 1$, the choice of $\kappa = 1$ yields both $\lambda = 0.5$ and $r_a = 4$. The linear stability curves are shown in Fig. 1. Both the double-zero and subcritical Lorenz Hopf bifurcations exist and the unstable limit cycle, bifurcating from R_c for $\beta = 0$, terminates at the double-zero point and so corresponds to the Hopf bifurcation of the nontrivial equilibria, discussed in Sec. 3.3 above. In addition there are curves of steady and Hopf bifurcation, associated with the trivial equilibrium.

The interested reader might compare this case with that of Fig. 1 in [Hide & Moroz, 1999], which shows the linear stability curves (as well as summarizing the nonlinear dynamics) for the original [Hide *et al.*, 1996] dynamo, modified by the presence of an azimuthal eddy current. As discussed by Hide

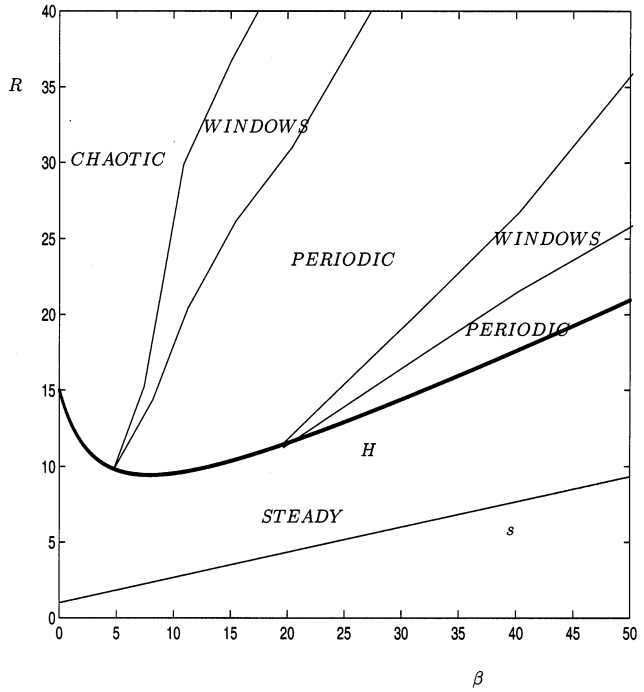

Fig. 2. As in Fig. 1 but for case (ii) and with $\Lambda = 1.2$.

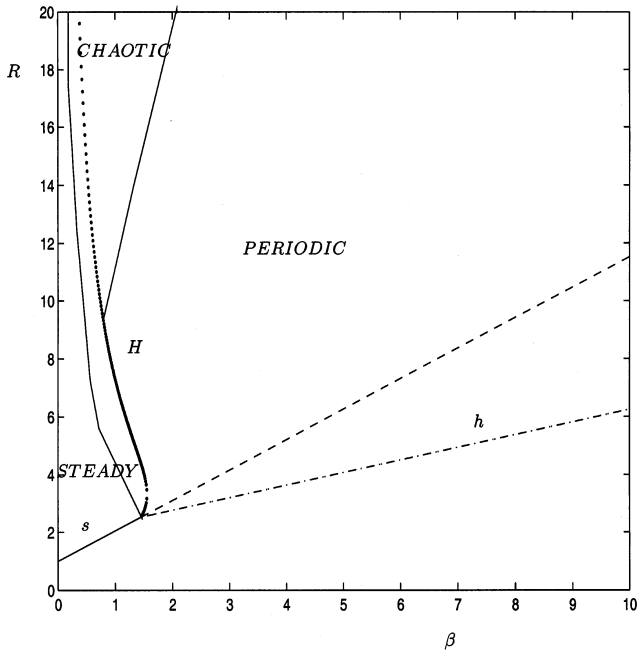

Fig. 3. As in Fig. 1 but for case (iii) and with $\sigma = 1.9$.

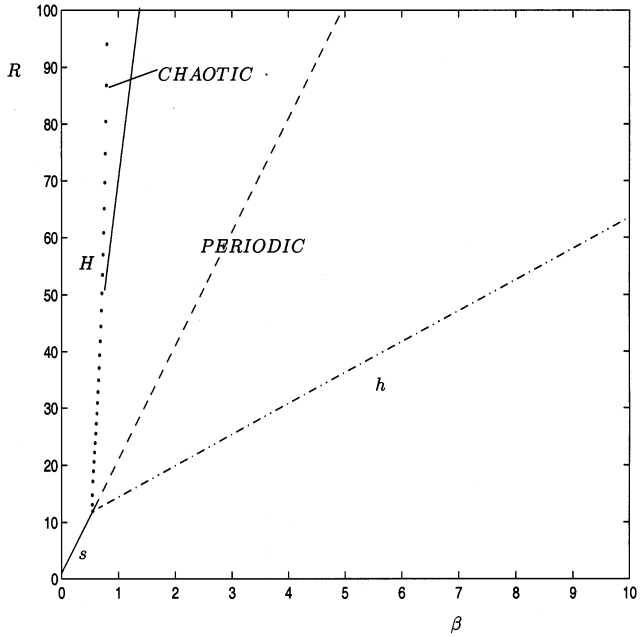

Fig. 4. As in Fig. 3 but with $\sigma = 0.1$.

and Moroz [1999], the $\beta \to 0$ limit of their model yields the Lorenz equations, as is the case here for the extended Malkus–Robbins dynamo. The two subcritical Hopf bifurcations, which occur on the $\beta = 0$ axis, are therefore equivalent. Indeed most of the cases in this subsection have their counterparts in the [Hide & Moroz, 1999] study.

3.4.2. $\Lambda > 1$ *and* $\sigma > 1 + \nu$

Figure 2 shows an example of the case $\Lambda > 1$ and $\sigma > 1 + \nu$, where we have now taken $\Lambda = 1.2$ but have left σ, ν and κ (and so r_a) unchanged from Fig. 1. The double-zero condition is violated and so no limit cycles can bifurcate off the steady stability curve (which remains stable throughout). However the Lorenz subcritical Hopf bifurcation criterion (5) is still satisfied and so there is a limit cycle born.

These linear stability curves may be compared with those of Fig. 2 in [Hide & Moroz, 1999].

3.4.3. $\Lambda < 1$ *and* $0 < \sigma < 1 + \nu$

For $\Lambda < 1$ and $0 < \sigma < 1 + \nu$, we chose $\Lambda = 0.5$, $\nu = 1$, $\kappa = 1$ and $\lambda = 0.5$ as in case (i) above, but considered several different values for σ (and so r_a). Here we present the linear stability curves for $\sigma = 1.9$ and $\sigma = 0.1$ (see Figs. 3 and 4 respectively). In both cases the double-zero bifurcation exists, but not the Lorenz subcritical Hopf bifurcation at $\beta = 0$. Therefore the (subcritical) limit cycles which bifurcate off the nontrivial equilibria no longer terminate at R_c.

Here we can compare the linear stability curves with those of Fig. 5 in the original [Hide *et al.*, 1996] dynamo (see also Fig. 3 of [Hide & Moroz, 1999]).

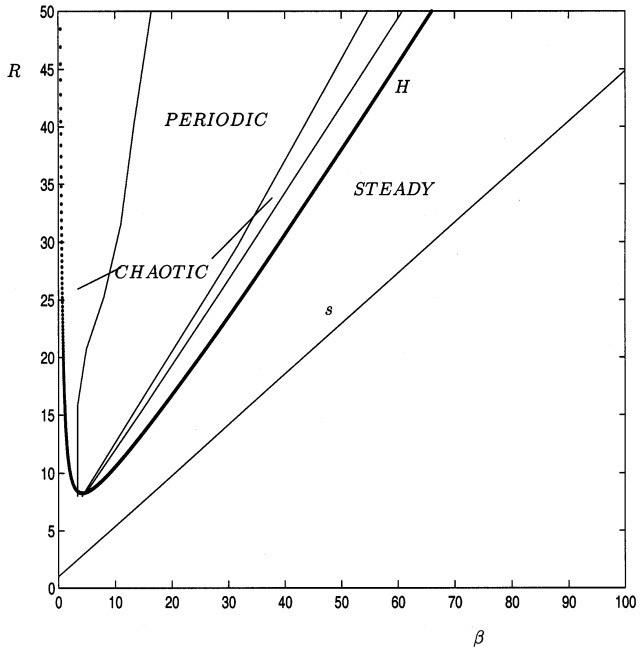

Fig. 5. As in Fig. 2 but for case (iv) with $\sigma = 1.9$.

3.4.4. $\Lambda > 1$ *and* $0 < \sigma < 1 + \nu$

Finally, we consider the case of $\Lambda > 1$ and $0 < \sigma < 1 + \nu$. Neither R_c nor the double-zero bifurcation exist. Figure 5 shows the linear stability curves for $\Lambda = \lambda = 1.2$, $\nu = \kappa = 1$ and $\sigma = 1.9$. Other choices for σ which are consistent with these inequalities yield similar results. The linear stability curves for this final case do not appear to have any counterparts in the [Hide *et al.*, 1996] class of dynamo models and so can be viewed as a new feature that appears in the extended Malkus–Robbins system.

Numerical calculations using (21) and (22) yield a nontrivial Hopf bifurcation curve, despite the absence of R_c and the double-zero bifurcation. The existence of oscillatory solutions has been verified by direct numerical integrations of (8) (see the next section).

4. Numerical Investigations

In the previous section we presented the linear stability analysis for (8), culminating in figures depicting the linear stability curves. In this section we describe the results of numerical integrations of (8), comparing wherever appropriate with behaviors found in the other studies of low-order dynamos. As well as phase portraits and/or time series for selected parameter values, we shall also display our results as plots of the local maximum amplitude of the oscillatory solutions (which arise through Hopf bifurcations) as functions of one of the control parameters β and R. This latter approach, used to good effect in [Moroz, 2001a], yields a transition sequence which indicates where chaotic, periodic and multiple-periodic solutions might be found. In all of our integrations, $\nu = r_r = 1$, while the other parameters were permitted to vary, depending upon which case was under consideration.

4.1. $\Lambda < 1$ *and* $\sigma > 1 + \nu$

As well as a depiction of the linear stability curves for $\Lambda = 0.5$, $\sigma = 5$ and $\nu = 1$ (as a typical example of the first case we discussed above), Fig. 1 also shows transition boundaries between steady, periodic and chaotic solutions. Although the scenario in Fig. 1 resembles that of Fig. 1 in [Hide & Moroz, 1999], the two cases differ in one respect. While the region of chaotic solutions extends to the left of the Hopf bifurcation curve that links R_c with the double-zero bifurcation point d (as in [Hide & Moroz, 1999], numerical integrations of (8) show that transition occurs via period-doubling bifurcations rather than through the intermittent destabilization of a periodic trajectory (as in [Hide & Moroz, 1999]). In addition, not only does the region of chaotic solutions extend to the left of the nontrivial Hopf bifurcation curve H, but there is also a region of stable periodic solutions in the neighborhood of the double-zero point (see Fig. 1). This bifurcation picture is also more intricate than the one found by Hide *et al.* [1996], where chaos was confined to a much smaller region of parameter space in the (β, α)-plane.

We have investigated the effects of hysteresis on the location of the two nonlinear transition curves shown in Fig. 1. Figures 6(a) and 6(b) show the hysteresis for $\beta = 2.3$ when R is increased and decreased respectively. There are a number of different coexisiting steady and oscillatory states. Firstly the small region of chaotic states at the transition between steady and oscillatory solutions when R is decreased [Fig. 6(b)] co-exists with steady states when R is increased [Fig. 6(a)] for $4.83 < R < 5$. Then a simple periodic state [Fig. 6(b)] coexisits with the steady solution for $5 < R < 6.7$.

The transition between chaotic, asymmetric and symmetric periodic solutions is also subject to hysteresis. When R is increased, the symmetric periodic solution loses stability to an asymmetric

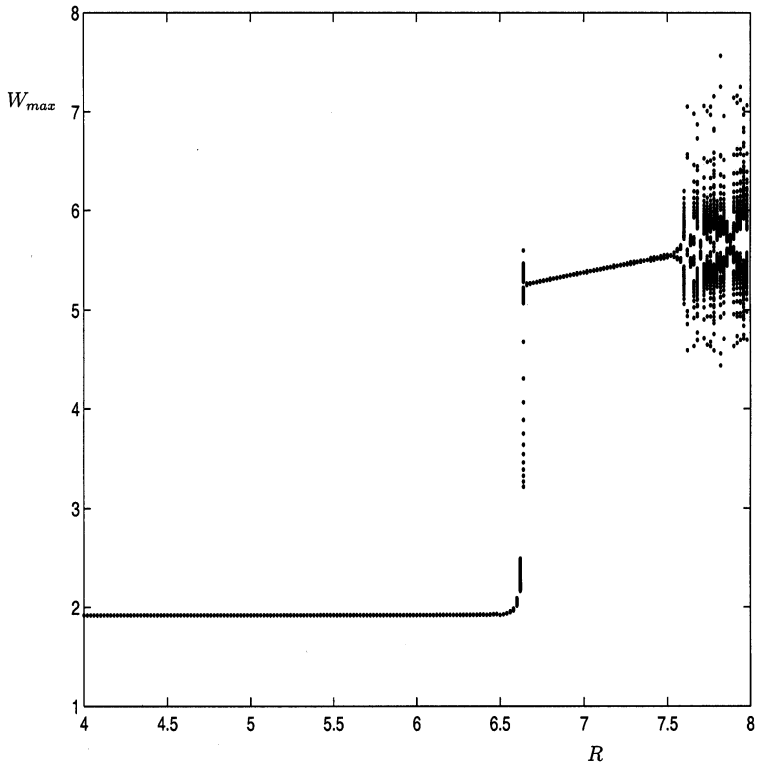

(a)

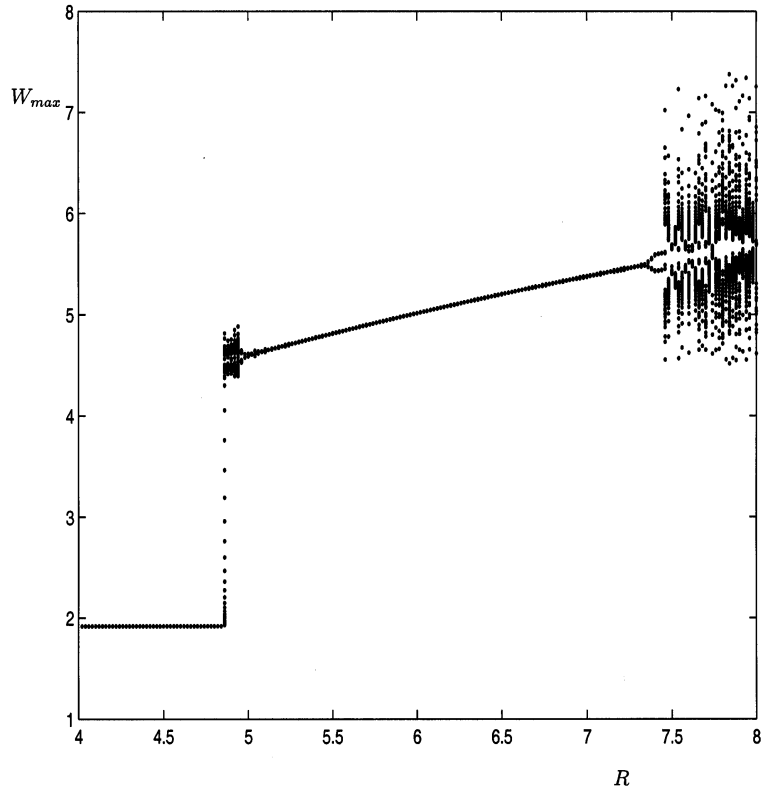

(b)

Fig. 6. Plot of the local maximum values of $W(t)$ as a function of R for case (i) when $\beta = 2.3$ and R is increased. (b) As in (a) but when R is decreased.

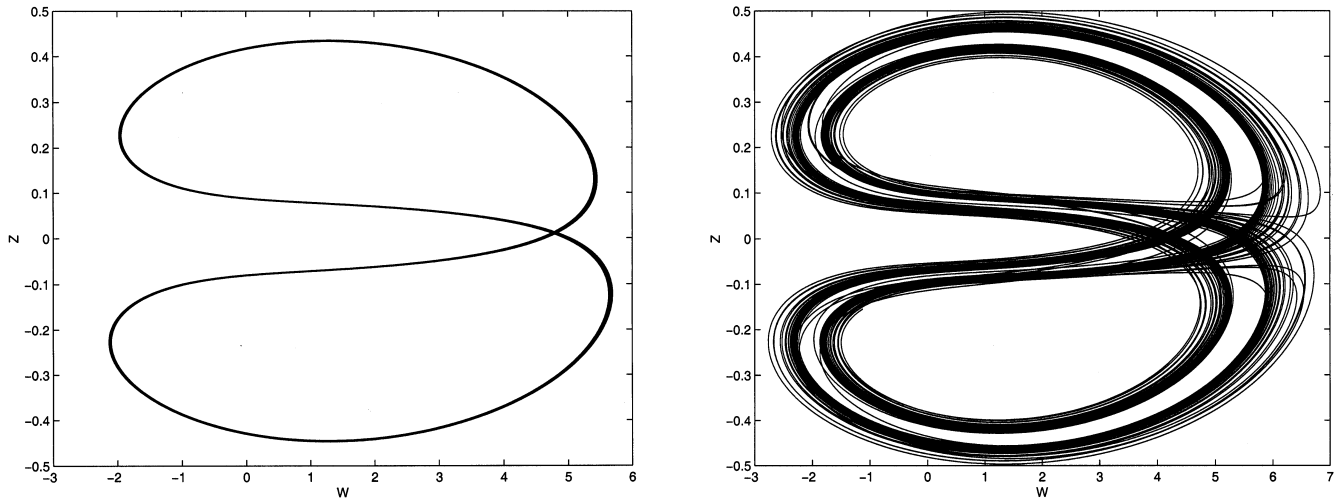

(a) (b)

Fig. 7. Phase portrait in the (W, Z)-plane for $\beta = 2.3$ and $R = 7.5$ when R is increased through this value. (b) As in (a) but when R is decreased.

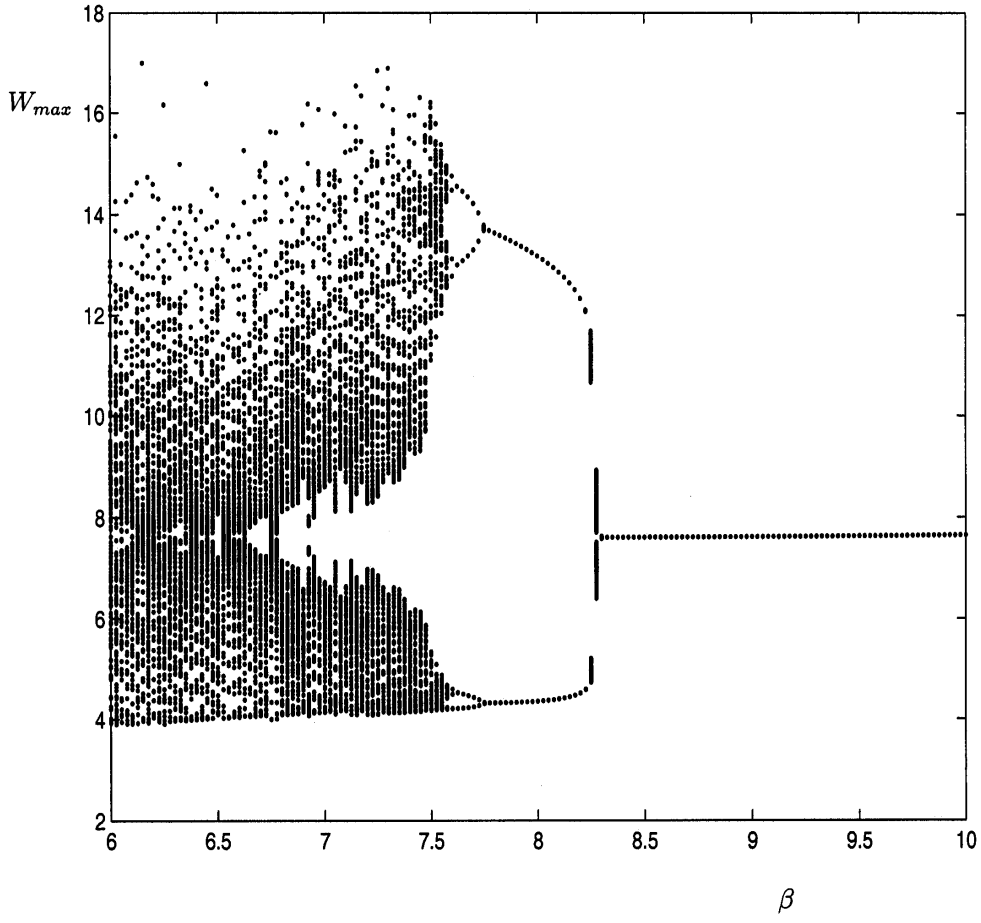

(a)

Fig. 8. Plot of the local maximum values of $W(t)$ as a function of β for case (i) when $R = 20$ and β is increased. (b) As in (a) but when β is decreased.

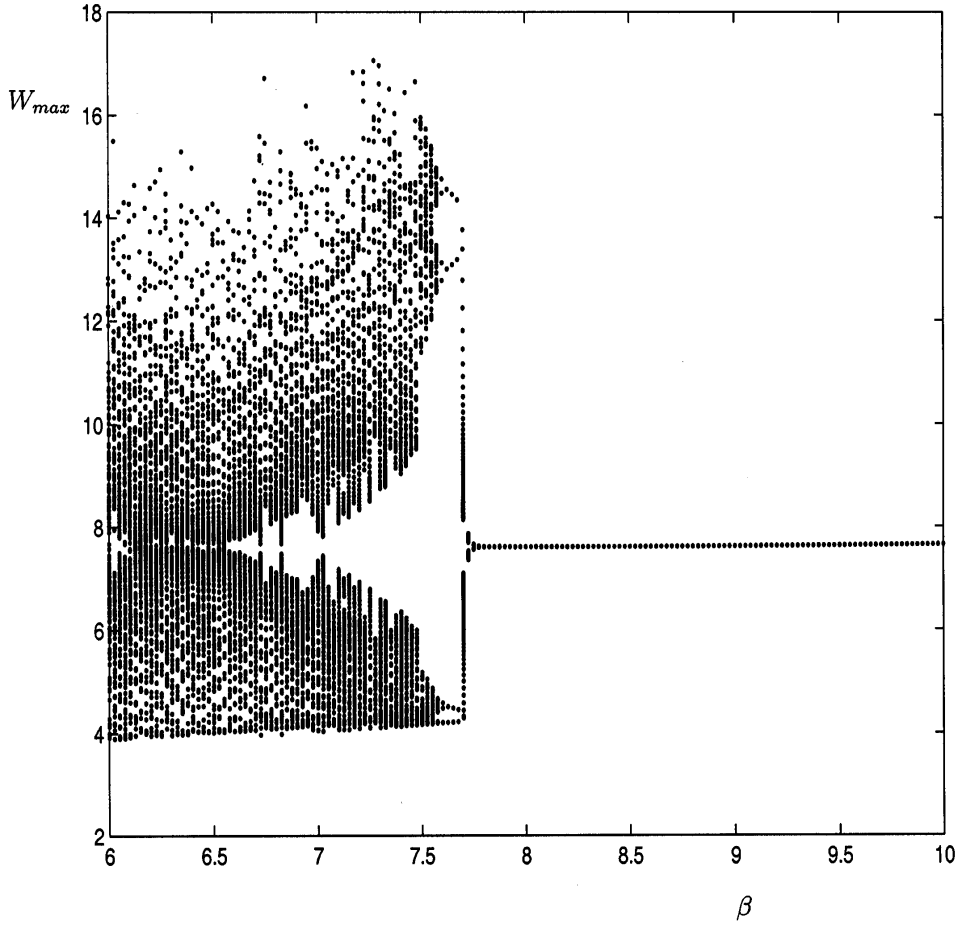

(b)

Fig. 8. (*Continued*)

orbit for $R \approx 7.4$ and then to chaotic behavior for $R \approx 7.6$, while when R is decreased the transition from chaotic to asymmetric behavior occurs for $R \approx 7.48$ and the transition which restores the symmetry of the limit cycle occurs for $R \approx 7.34$. Figures 7(a) and 7(b) show the (W, Z) phase portraits for $\beta = 2.3$ and $R = 7.5$. When R is increased through this value [Fig. 7(a)] we observe an asymmetric periodic orbit, but when R is decreased [Fig. 7(b)], we observe a noisy period-two cycle.

Hysteresis is also observed if we fix R but vary β. Figure 8(a) shows the transition sequence for $R = 20$ when β is increased, while Fig. 8(b) shows the corresponding scenario for decreasing β. In the latter case, the first loss of stability of the limit cycle is directly to a period-two cycle at $\beta \approx 7.75$ (see Fig. 9(a) for $\beta = 7.65$), which then loses stability to a period-four cycle at $\beta \approx 7.6$ [see Fig. 9(b)]. When β is increased, however, the period-two orbit loses stability at $\beta \approx 7.75$ to an asymmetric limit cycle before the restoration of symmetry at $\beta \approx 8.27$.

4.2. $\Lambda > 1$ and $\sigma > 1 + \nu$

The case of $\Lambda = 1.2$ and $\sigma = 5$, with $\nu = 1$, provides one of the more interesting nonlinear scenarios considered in this study. If β is held fixed and R varied or if R is kept fixed and β varied, we observe a rich interleaving of periodic and chaotic solutions, with period doubling cascades, windows of periodic solutions, separated by regions of chaotic solutions, as well as simple steady state solutions.

Hysteresis is again observed along the Hopf stability curve, being more marked when the transition is between steady and chaotic solutions than between steady and periodic. There did not appear to be any hysteresis involving other transitions. For example, when $\beta = 0.01$, chaotic behavior is ob-

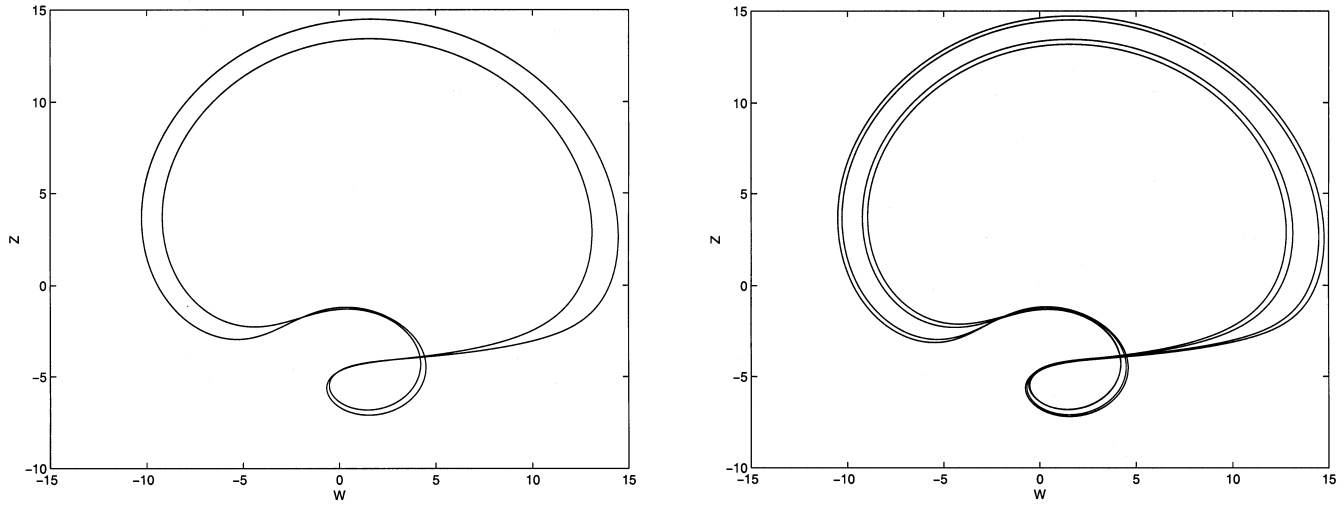

(a) (b)

Fig. 9. Period-two cycle for case (i) with $R = 20$ and $\beta = 7.65$ when β is decreased through this value. (b) Period-four cycle for $R = 20$ and $\beta = 7.6$ when β is decreased through this value.

served for $15.25 < R < 40$ (the upper value for R considered for this case) when R is increased and for $14.25 < R < 40$ when R is decreased. The transition from chaotic behavior is directly to steady state solutions.

Because of the richness of solutions in this case, as well as depicting some approximate transition boundaries in Fig. 2, we also present a selection of transition curves of $W_{\max}$ as functions of β with R held fixed or vice versa. With β held fixed and R varied, chaotic solutions predominate for $0 \leq \beta \leq 5$ with a barely discernable window of periodic solutions for $\beta = 5$ and $31.85 < R < 32.05$. When $\beta = 7.5$, there is a small band of chaotic states at the linear stability boundary, giving way to a simple periodic solution for $10 < R < 15.3$. Windows of periodic states, interleaving regions of chaotic behavior then appear. Figure 10(a) shows the scenario for $\beta = 10$. When $\beta = 20$ [Fig. 10(b)], nearly all of these periodic windows have disappeared, while for $\beta = 30$ periodic solutions predominate. There is still a small region of chaotic solutions away from the Hopf stability boundary, which gives rise again to interleaving of periodic and chaotic states for $\beta = 40$ and $\beta = 50$ (see Fig. 11).

Similar intricate behavior can be found when R is held fixed and β is varied. Figure 12 shows the transition sequence for $R = 25$.

In contrast to the first case described above, therefore, the region of parameter space for the existence of oscillatory solutions covers a wider range of values of β and much smaller values of α than in [Hide & Moroz, 1999].

4.3. $\Lambda < 1$ and $0 < \sigma < 1 + \nu$

When $\Lambda = 0.5$, $\sigma = 1.9$ and $\nu = 1$, the region of parameter space occupied by chaotic solutions is now greatly reduced, compared to the above two cases. There is again a marked hysteresis involving the location of the steady-chaotic and the steady-periodic transition to the left of the nontrivial Hopf bifurcation curve. For example when $\beta = 1.0$, the transition from steady to periodic occurs at $R \approx 7.4$ when R is increasing, whereas the opposite transition from periodic to chaotic occurs at $R \approx 5$ when R is decreasing. There is also hystersis at the periodic–chaotic boundary to the right of the nontrivial Hopf curve, but this is less marked, with transition values differing by only 0.1 or 0.2.

When $\sigma = 0.1$, with all the remaining parameters kept the same, the (β, R)-plane is dominated by simple periodic or steady solutions, with chaos being confined to an initially narrow band close to the nontrivial Hopf bifurcation curve, this narrow band broadening out for larger values of R.

4.4. $\Lambda > 1$ and $0 < \sigma < 1 + \nu$

For the final case, we took $\Lambda = 1.2$, $\nu = 1$ and $\sigma = 1.9$. Although neither R_c nor the double-zero bifurcation exist, the nontrivial equilibrium states

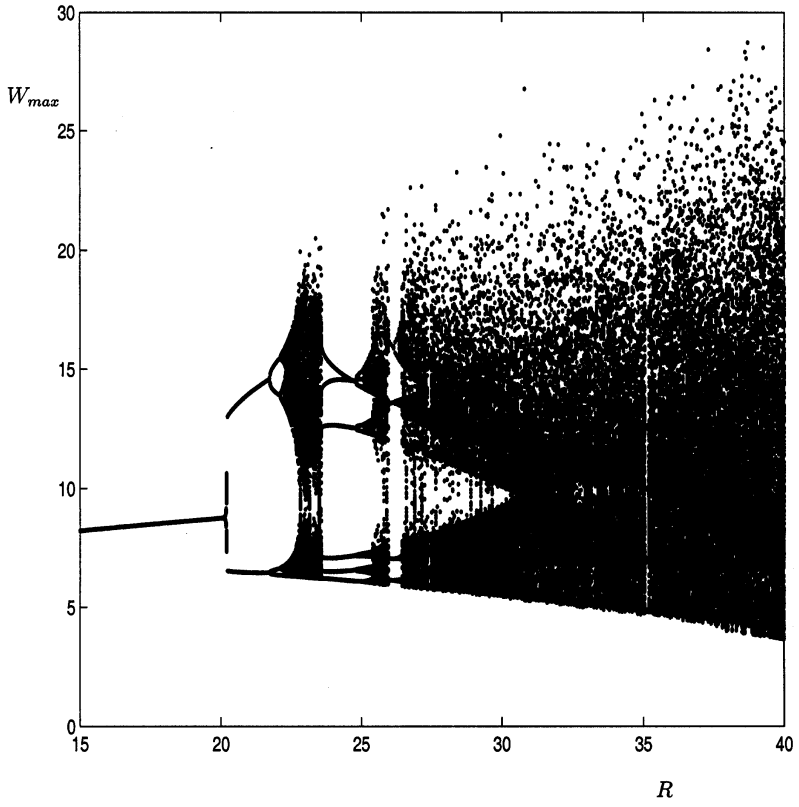

(a)

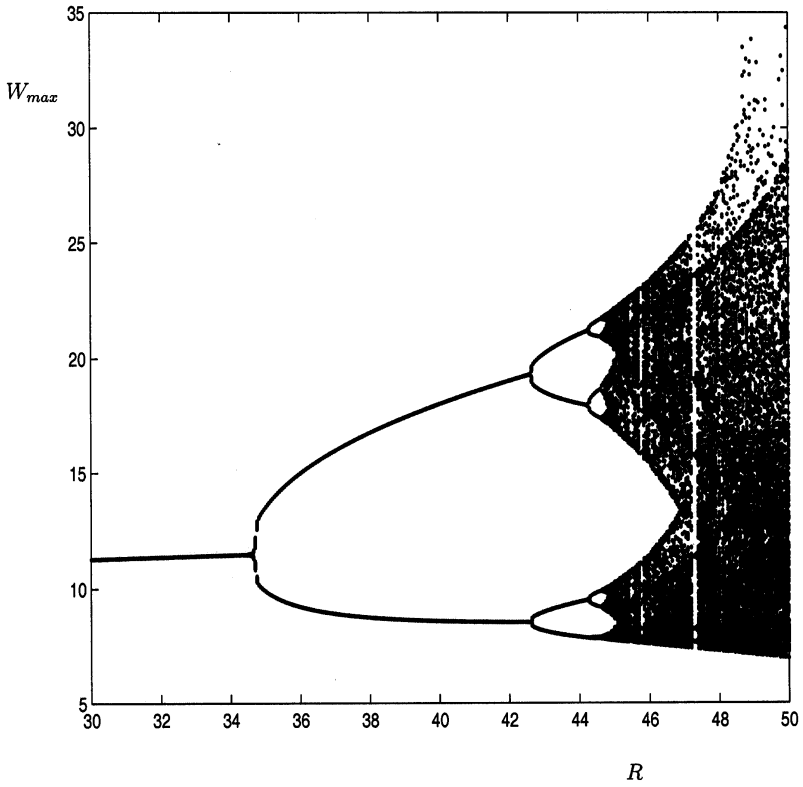

(b)

Fig. 10. (a) Bifurcation transition sequence for case (ii) with R increasing for $\beta = 10$. (b) As in (a) but for $\beta = 20$.

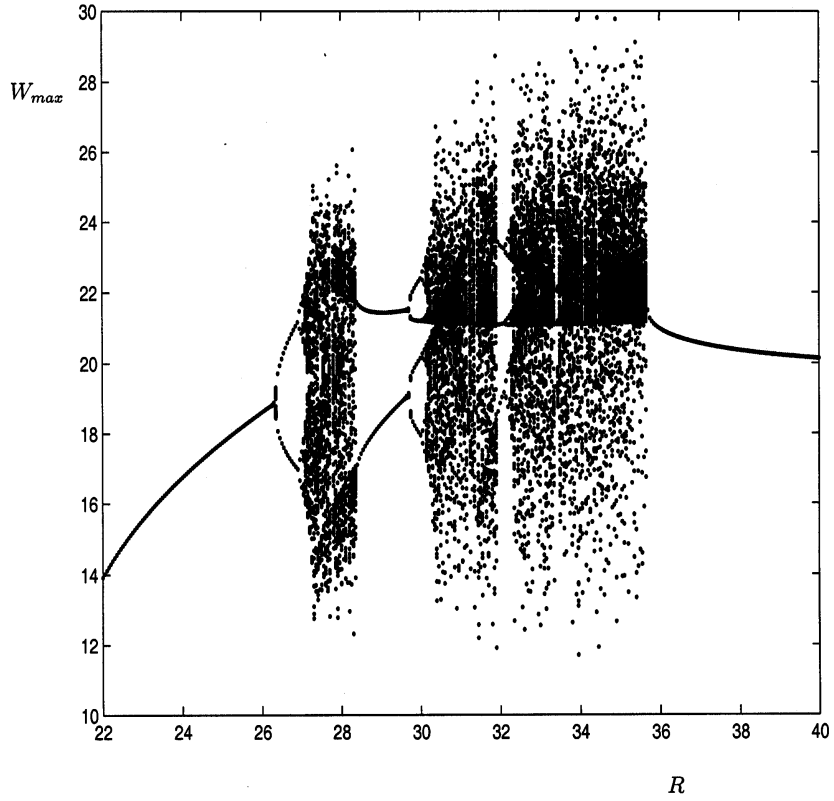

Fig. 11. As in Fig. 10(a) but for $\beta = 50$.

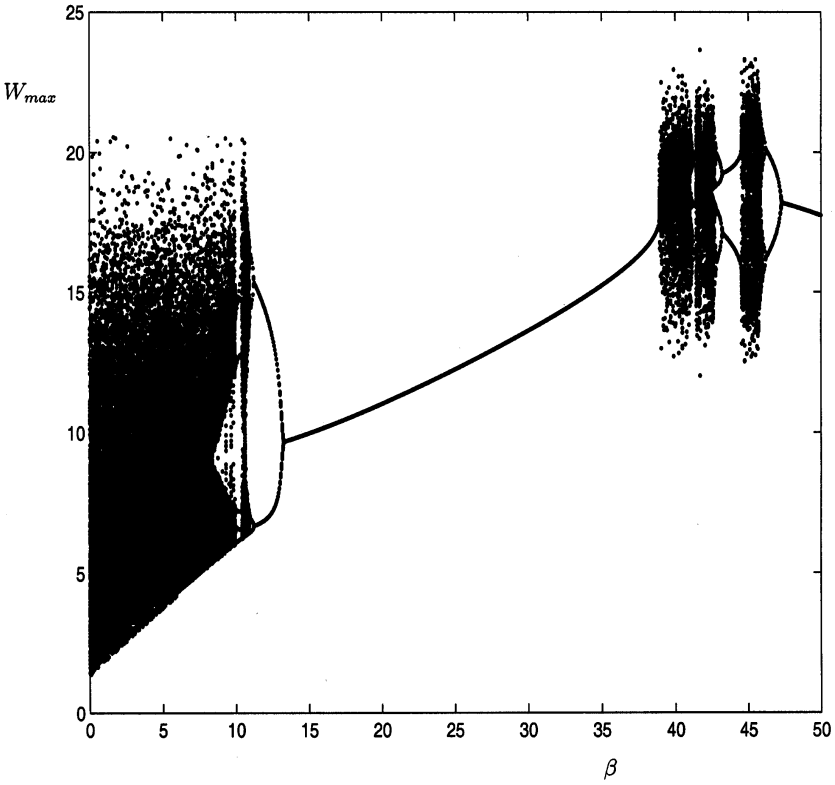

Fig. 12. Bifurcation transition sequence for case (ii) with β increasing and $R = 25$.

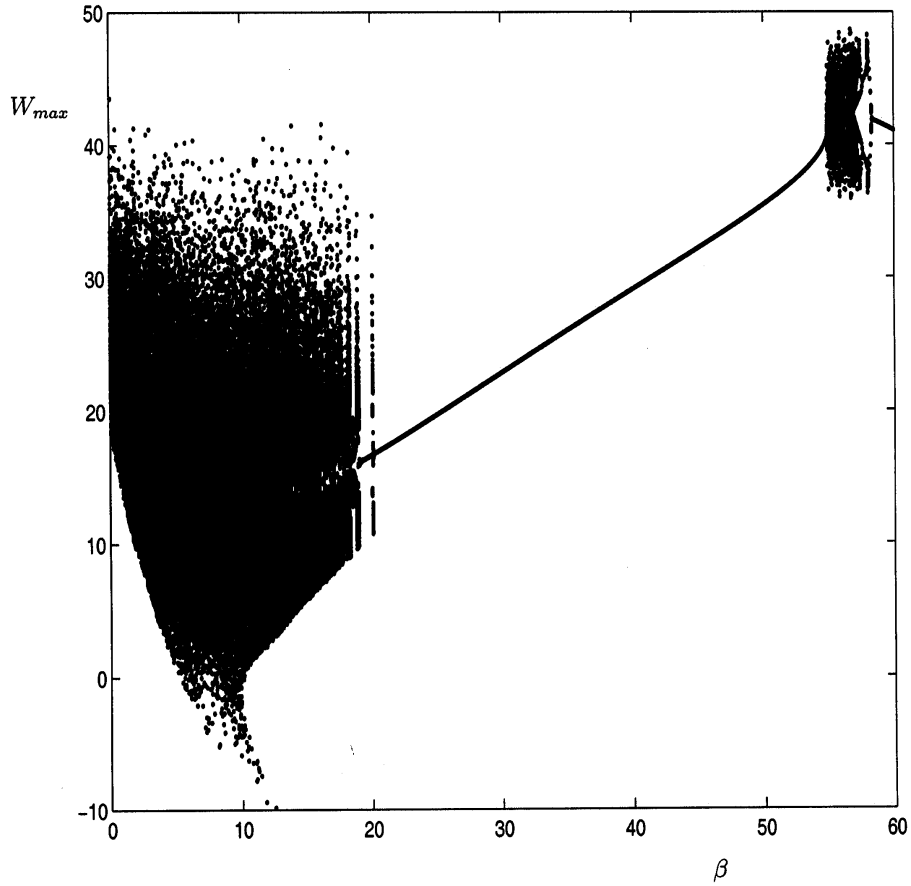

Fig. 13. Bifurcation transition sequence for case (iv) for $R = 50$ and $0 < \beta < 60$.

undergo Hopf bifurcations and numerical integrations reveal two regions of chaotic behavior, separated by regions of periodic behavior. As in the previous cases, chaos is found near the left-hand Hopf stability boundary, marking the transition to steady state solutions. It is also found close to the right-hand boundary, being separated from the steady states by a small region of periodicity, which increases as R and β increase. Figure 13 shows the transition sequence for $R = 50$ for $0 < \beta < 60$.

5. Discussion

In this paper we have investigated an extension of the celebrated Malkus–Robbins dynamo, which features as a special limit of one of the hierarchy of self-exciting coupled Faraday-disk homopolar dynamos proposed by Hide [1997]. We have identified and studied four cases of interest which allow or forbid certain key bifurcations. Moreover we have compared the behaviors obtained for these cases with those found in the original Malkus–Robbins dynamo as well as in some of the other self-exciting dynamo models.

The presence of a linear series motor greatly enriches the range of possible behaviors in the Malkus–Robbins dynamo to include not only codimension-one Hopf bifurcations for both the trivial and the nontrivial equilibria but also the codimension-two double-zero bifurcation which is a characteristic feature of the Hide *et al.* [1996] family of dynamos. There are extensive regions of chaotic and periodic states with interleaving between the two in the form of windows of periodicity and chaos. There is also evidence for hysteresis in the neighborhoods of some of the linear and nonlinear transition boundaries between steady, periodic and chaotic solutions, with coexistence of different types of finite amplitude states for the same parameter values.

The special limit of Case 3 of [Hide, 1997] considered here is one of the simplest reductions of this third class of dynamo and represents a first step in its analysis. In future work we will build upon

the results of this paper and restore some of the neglected components of Case 3 to investigate the effects of their reinclusion.

Acknowledgment

We are grateful to Prof. R. Hide for useful discussions.

References

Goldbrum, P., Moroz, I. M. & Hide, R. [2000] "On the biasing effect of a battery on a self-exciting Faraday disk homopolar dynamo loaded with a linear series motor," *Int. J. Bifurcation and Chaos* **10**, 1875–1885.

Hide, R. Skeldon, A. C. & Acheson, D. J. [1996] "A study of two novel self-exciting single-disk homopolar dynamos: Theory," *Proc. R. Soc. Lond.* **A452**, 1369–1395.

Hide, R. [1997] "The nonlinear differential equations governing a hierarchy of self-exciting coupled Faraday-disk homopolar dynamos," *Phys. Earth Planet. Interiors* **103**, 281–291.

Hide, R. [1998] "Nonlinear quenching of current fluctuations in a self-exciting homopolar dynamo," *Nonlin. Processes in Geophys.* **4**, 201–205.

Hide, R. & Moroz, I. M. [1999] "Effects due to induced azimuthal eddy currents in the self-exciting Faraday disk homopolar dynamo with a nonlinear series motor: I. Two special cases," *Physica* **D134**, 387–301.

Malkus, W. V. R. [1972] "Reversing Bullard's dynamo," *E.O.S. Trans. Amer. Geophys. Un.* **53**, 617.

Moroz, I. M., Hide, R. & Soward, A. M. [1998a] "On self-exciting coupled Faraday disk homopolar dynamos driving series motors," *Physica* **D117**, 128–144.

Moroz, I. M., Smith, L. A. & Hide, R. [1998b] "Synchronised chaos in coupled double disk homopolar dynamos," *Int. J. Bifurcation and Chaos* **8**, 2125–2133.

Moroz, I. M. & Hide, R. [2000] "Effects due to induced azimuthal eddy currents in the self-exciting Faraday disk homopolar dynamo with a nonlinear series motor: II. The general case," *Int. J. Bifurcation and Chaos* **10**(12), 2701–2716.

Moroz, I. M. [2001a] "On the behaviour of a self-exciting Faraday disk homopolar dynamo with battery in the presence of an external magnetic field," *Int. J. Bifurcation and Chaos* **11**(6), 1695–1705.

Moroz, I. M. [2001b] "Self-exciting Faraday disk homopolar dynamos magnetic field," *Int. J. Bifurcation and Chaos* **11**(12), 2961–2975.

Moroz, I. M. [2001c] "Synchronised dynamics in three coupled Faraday disk homopolar dynamos," *Fluid Dynamics and the Environment: Dynamical Approaches*, ed. Lumley, J. L. (Springer-Verlag), pp. 225–238.

Robbins, K. A. [1997] "A new approach to sub-critical instability and turbulent transitions in a simple dynamo," *Math. Proc. Cambridge Philos. Soc.* **82**, 309–325.

Skeldon, A. C. & Moroz, I. M. [1998] "On a codimension three bifurcation arising in dynamo theory," *Physica* **D117**, 117–127.

Appendix A: Derivation of the Hopf Bifurcation Curve for the Nontrivial Equilibrium Solutions

We can rewrite (20) as

$$B_0 = a_0 R + a_1 W_e \,, \tag{A.1a}$$

$$B_1 = b_0 W_e + b_1 R + B_2 R/W_e \,, \tag{A.1b}$$

$$B_2 = c_0 + c_1 W_e + R/W_e \,, \tag{A.1c}$$

$$B_3 = d_0 \,, \tag{A.1d}$$

where

$$a_0 = 2\sigma\Lambda, \quad a_1 = -a_0\nu \,, \tag{A.2a}$$

$$b_0 = \sigma\nu(\Lambda - 2), \quad b_1 = \sigma,$$

$$b_2 = (\sigma + \Lambda) \,, \tag{A.2b}$$

$$c_0 = (1+\nu)(\sigma+\Lambda), \quad c_1 = \sigma(\Lambda - 1) \,, \tag{A.2c}$$

$$d_0 = 1 + \nu + \sigma + \Lambda \,, \tag{A.2d}$$

so that the Hopf bifurcation curve (21) is calculated from the positive real root(s) of

$$AR^2 + BR + C = 0 \,, \tag{A.3}$$

where

$$A = b_1^2 + b_1(2b_2 - d_0)/W_e + b_2(b_2 - d_0)/W_e^2, \tag{A.4a}$$

$$B = b_2(2b_0 - d_0 c_1) + d_0(d_0 a_0 - c_0 b_1 - b_0) - d_0 c_0 b_2/W_e + b_1(2b_0 - d_0 c_1)W_e \,, \tag{A.4b}$$

$$C = d_0(d_0 a_1 - c_0 b_0)W_e + b_0(b_0 - d_0 c_1)W_e^2. \tag{A.4c}$$

Substitution of the admissible values for R into (20) and (22) then provides the corresponding values of the frequencies.